

LEO Capacity Modeling for Sustainable Design

Mark A. Sturza, Mark D. Dankberg, William N. Blount
Viasat, Inc.

ABSTRACT

LEO is a finite resource and “rivalrous” (each consumer reduces the amount available to others), yet available to all, incentivizing a “tragedy of the commons”. Current trends risk a global loss of access to space for decades or even centuries. If a fraction of the proposed mega-constellation satellites are deployed, there may be more than an order of magnitude increase in number of satellites, aggregate mass, and aggregate cross-sectional area in LEO. Orbiting satellites increasingly are at risk of being fragmented by collisions with debris. The accumulation of debris in LEO is one of the most pressing threats to the safety and sustainability of space exploitation. Attempts to slow debris growth have consisted of ad hoc, heuristic, guidance for new missions. We propose a holistic model using a multi-dimensional state vector approach to evaluate a “carrying capacity” metric, the sustainable satellite population distribution in LEO.

We consider carrying capacity to be the point at which the rate that satellites are consumed by collisions is equal to a specified fraction of the constant rate at which satellites are launched to maintain a constellation. This metric is used to explore the sensitivity to initial conditions, parameters, and constellations competing for access to carrying capacity, with interesting results. Namely: 1) removing the existing population of derelict rocket bodies does not result in a material increase in LEO carrying capacity, 2) the proposed second-generation configurations of two particular mega-constellation would consume all, or nearly all, of the carrying capacity in orbits neighboring those occupied by the constellations, and 3) less massive satellites facilitate greater carrying capacity.

Policy implications include highlighting the need for 1) orbital admittance control and minimum satellite reliability standards (i.e., using license conditions to limit the number of satellites, mass, and cross-sectional area, and requiring minimum satellite reliability standards), 2) suitable orbital regimes to support different types of systems, such as non-propulsive satellites, mega-constellations, and small constellations, and 3) a methodology for obtaining useful quantitative results regarding containing net debris growth and prioritizing effective interventions instead of intuitive heuristics and remediations currently being contemplated.

1. INTRODUCTION

In 2018, the United States (US) Federal Communications Commission (FCC) initiated a rulemaking on Orbital Debris Mitigation (ODM) which plainly addresses risks in the “New Space Age” posed by debris objects in low-Earth orbit (LEO) [1]. The FCC rulemaking notes that LEO is a finite resource and “rivalrous” (each consumer reduces the amount available to others), yet available to all, incentivizing a “tragedy of the commons”, such that the short-term economic interest of certain satellite operators could override larger, global interests in ensuring safe and sustainable access to space by all for generations.

At the start of 2022, there were around 6,000 satellites in LEO, with an approximate aggregate mass of 2.2 million kg and cross-sectional area of 37,000 m² [2]. In 2021 alone, the International Telecommunication Union (ITU) received filings for more than 1 million additional LEO satellites [3]. Even if only a fraction of these satellites are deployed, the result will be more than an order of magnitude increase in the number of satellites, aggregate mass, and aggregate cross-sectional area in LEO.

Once satellites are in orbit, they are at risk of being disabled or fragmented by collisions with debris. The growth of debris in Earth’s orbits is one of the most pressing threats to the safety and sustainability of space exploitation. The risk of collisions with debris resulting in the generation of further debris, and ultimately leading to a Kessler syndrome [4] of cascading, self-generating collisions, is one of the main costs. This ecological tipping point may render certain orbits unusable for decades, centuries, or even millennia. The potentially significant growth of lethal trackable (LT) and lethal non-trackable (LNT) debris has prompted rough estimates of when regions of LEO may become unusable in the absence of new interventions [5].

So far, attempts to slow net debris growth have consisted of ad hoc, heuristic, guidance for new missions [6]. Examples include minimizing intentional debris creation, improving tracking precision, incentivizing maneuverability, and improving post mission disposal reliability and timeframes. While helpful, these mitigations only address individual missions or constellations, or do not address all risk, including the interactions among all systems and debris contributing to debris propagation. Moreover, it has been unknown which, if any, of these types of interventions is most likely to result in a meaningful reduction in the rate of net debris growth.

Even though LEO is large, it is still finite and cannot support an unlimited number of satellite systems, even if each system individually complies with best practices. There are no comprehensive models or metrics considering all forms of debris propagation, extrapolating those effects into the future, and comparing effectiveness of candidate heuristic mitigations. Prior work includes [5], where a simple rate model was used to explore the collision rates that might occur with a large constellation, develop scaling relations to identify orbital density limits, and estimate the threshold for serious harm to the environment as 40,000 satellites at 600 km altitude and 1,000 satellites at 1200 km.

We propose a methodology, and metric, using a comprehensive multi-dimensional state vector and extrapolating that state vector into the future. The methodology models debris population evolution due to interactions of maneuverable and non-maneuverable objects given key physical characteristics, such as, orbits, mass, cross sectional area, and area-to-mass ratio for trackable objects such as satellites, rocket bodies, and LT debris, as well as estimated equivalent distributions for LNT debris.

This paper attempts to facilitate: 1) quantitatively measuring absolute and relative effectiveness of candidate regulations and policies governing space access and operations, and remediations such as debris removal strategies, 2) reframing the problem to consider interactions among all missions and constellations, instead of merely addressing each one individually and based on historical debris flux models, and 3) fostering identification of quantitative system design characteristics that slow, halt, or reverse acceleration towards a point in time when access to space is intolerably impaired or even lost.

A metric is used to estimate the LEO “carrying capacity”, that is, the sustainable satellite population distribution in LEO. The proposed approach better estimates future debris propagation because it encompasses both existing debris, and the likelihood that non-debris objects become debris within a given time horizon. The performances of mitigations, such as Space Surveillance and Tracking (SST), Space Situational Awareness (SSA), and Space Traffic Management (STM) are accounted for in the metric computation. This methodology enables comparing holistic global contributions to debris propagation as a function of specific system characteristics and deducing the incremental impact of individual systems and characteristics on LEO carrying capacity.

2. CARRYING CAPACITY

The term “carrying capacity” was used by Mark Twain to describe the maximum loads of people and goods that could be accommodated on a steamboat [7]. In the 1960’s, “carrying capacity” was used with respect to the number of astronauts in a spaceship, and then for sustainable global population [8]. It has also been used for the debris load that an orbit can hold [9]. More recently, “carrying capacity” has been used to describe the maximum sustainable population of satellites that the space environment can support [10, 11, 12, 13, 14, 15, 16, 17].

To analyze the impact of a satellite constellation on the carrying capacity of LEO, we define a residual carrying capacity (RCC) for a given satellite configuration which quantifies the number of additional satellites, with a specified configuration, that can be sustained in conjunction with the existing orbital objects and new constellations competing for RCC.

Consider a simple scalar model for the evolution of a population of LEO satellites

$$\frac{\partial S}{\partial t} = \frac{1}{\zeta} s - \frac{1}{\zeta} S - \mathcal{R}(S, t)$$

where ζ is the design lifetime of each satellite, s/ζ is the launch rate, and $\mathcal{R}(S, t)$ is the collision rate. The collision rate term includes the effects of the existing orbital objects (the background), new constellations competing for RCC, and the constellation under test.

At equilibrium, the derivative is zero, giving

$$S_{eq} = s - \zeta \mathcal{R}(S_{eq}, t)$$

Note that when $\mathcal{R}(S_{eq}, t)$ is nonzero, to maintain equilibrium for a constellation with S_{eq} satellites, additional satellites must be launched to replace those lost through collisions. Limiting the number of replacement satellites, those launched to replace active satellites rendered passive (non-operational) or fragmented by collisions, to a fraction, δ , of the launch rate size, adds a constraint that

$$\mathcal{R}(S_{eq}, t) \leq \delta \frac{1}{\zeta} s$$

At equilibrium, however,

$$\mathcal{R}(S_{eq}, t) = \frac{1}{\zeta} s - \frac{1}{\zeta} S_{eq}$$

Which simplifies to

$$s(1 - \delta) \leq S_{eq}$$

In general, the RCC is then given by

$$S^* = \max_s S_{eq} \quad \text{subject to} \quad s(1 - \delta) \leq S_{eq}$$

Using the equilibrium population (assuming such an equilibrium even exists) is problematic as it requires finding the limit of the satellite population as t goes to infinity. Furthermore, the equilibrium population may tend to zero due to accumulation of debris in higher orbits. Instead, we use the pseudo-equilibrium point, \tilde{S}_{eq} , after a finite time T , “the finite-time RCC”, \tilde{S}^* . The maximization then becomes

$$\tilde{S}^* = \max_s \tilde{S}_{eq} \quad \text{subject to} \quad s(1 - \delta) \leq \tilde{S}_{eq}$$

If the RCC is exceeded, the runaway creation of debris can be faster than exponential [15], at which point it may be impossible to reverse runaway until all satellites are consumed by debris and atmospheric drag causes the decay of all debris in LEO. Depending on the orbits, this may take decades, centuries, or even millennia.

3. MODEL

A model is developed to explore the dependence of RCC on the various assumptions. Objects in orbit are divided into seven classes: Active Satellites (A), Active Probe Satellites (C), Passive Satellites (P), Passive Probe Satellites (Q), Derelict Rocket Bodies (R), LT Debris (D), and LNT Debris (E). The A objects are active satellites in orbit at initialization and those launched as part of constellations competing for carrying capacity. The P objects are passive satellites in orbit at initialization and those former A objects that have either failed PMD or have been rendered non-maneuverable by non-fragmenting collisions. The C objects are satellites launched to determine (i.e., probe) the RCC associated with a particular parameter set under consideration. The Q objects are former C objects that have either failed PMD or been rendered non-maneuverable by non-fragmenting collisions. The transition between LT and LNT debris depends on SST performance.

LEO is partitioned into N equal thickness shells, with the first shell starting at 200 km and the last shell ending at 2,000 km. The shell centers (m) are:

$$h_k = \left(k - \frac{1}{2}\right) \times \Delta h + 200,000$$

where the shell thickness (m) is given by:

$$\Delta h = \frac{2,000,000 - 200,000}{N}$$

Each class of objects is modeled by a $N \times 1$ state vector with elements for each of the orbital shells. The state vectors (**A**, **P**, **R**, **D**, and **E**) are nominally initialized from the SATCAT (objects in orbit) [18] with objects assigned by mapping mean altitude to shell, k . Payload objects that have been in orbit for less than the satellite design lifetime, ζ , are mapped to **A** (assuming they are maneuverable) and payloads that have been in orbit for a longer time are mapped to **P** (assuming they are non-maneuverable). Rocket bodies are mapped to **R** and debris to **D**. The LNT Debris (**E**) are initialized to a multiple of **D**. The active and passive satellite probe vectors, **C** and **Q**, are initialized to zero. The RCC is estimated by injecting probe satellites into each shell until RCC is reached.

Fig. 1 shows the population distribution as initialized from the SATCAT. The active SpaceX and OneWeb satellites can be seen around 550 km and 1,100 km, respectively. The debris peaks are around 500 km, 800 km, 1,300 km, and 1,450 km.

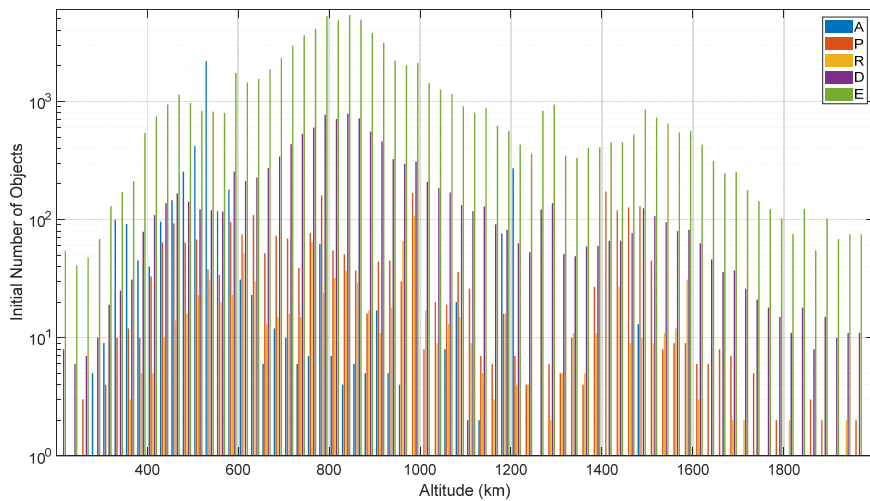


Fig. 1 – Initial SATCAT Population Distribution

The total non-maneuverable (P, R, D, E) mass (kg) and cross-sectional area (m^2) as a function of altitude are shown in Fig. 2. The peaks are seen to occur around 500 km, 600 km, 800 km, 1,000 km, and 1,450 km. These are altitudes where it is anticipated initializing with the SATCAT objects will have the most impact. The impact of the lower two will decrease with time due to drag, and that of the upper three will persist.

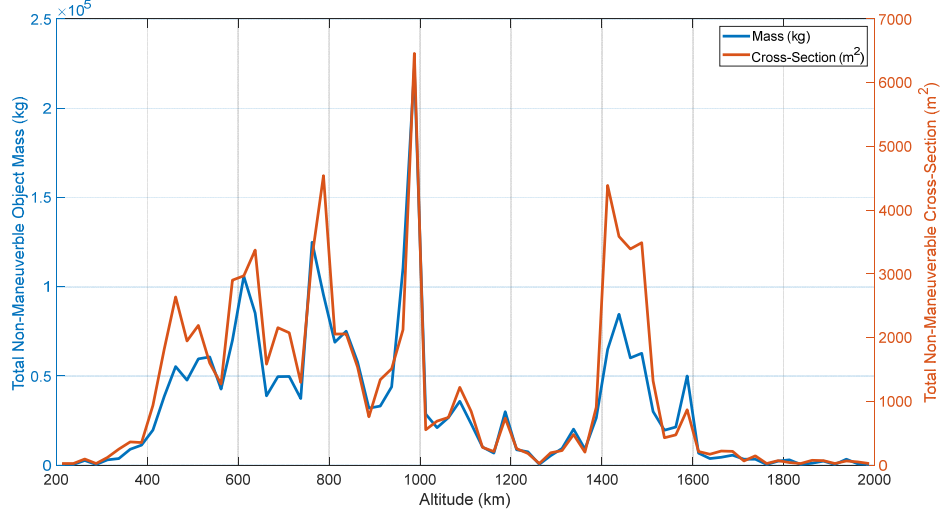


Fig. 2 – Aggregate Non-Maneuverable (P, R, D, E) Mass (kg) and Cross-Sectional Area (m^2) at Initialization

All orbits are modeled as circular. Active satellites (A and C) are assumed to be station-kept during design lifetime, ζ , and removed instantly at end of life when post-mission disposal (PMD) is successful (probability ρ) and converted to passive satellites (P and Q , respectively) if PMD is not successful (probability $1 - \rho$), no other failure mechanisms are modeled. A fixed probability of an active satellite not avoiding a collision, α , is modeled, with the probability of two active satellites colliding modeled as α^2 . Improving SSA and STM performance reduces the value of α . The probability of active satellites colliding with non-lethal, non-trackable (NLNT) debris resulting in loss of maneuverability is ignored. This is an optimistic assumption for RCC. Another optimistic assumption for RCC is that collisions between two LNT objects are assumed to remove those debris objects from the population, but not create any additional objects.

Fixed cross-sectional areas (m^2) are assumed for each object type. The cross-sectional area of the passive satellites is defined in terms of the cross-sectional area of the active satellites via

$$\sigma_P = \frac{1}{2} \sigma_A \quad \sigma_Q = \frac{1}{2} \sigma_C$$

where the factor of 1/2 accounts for the tumbling of passive satellites. The active and passive satellites are assumed to have the same mass, hence

$$m_P = m_A \quad m_Q = m_C$$

The LT and LNT debris are modeled as spherical with diameters d_{LT} and d_{LNT} , respectively, and with $2,000 \text{ kg} \cdot \text{m}^{-3}$ density, compared to $2,700 \text{ kg} \cdot \text{m}^{-3}$ for aluminum, a common material in satellite construction, giving

$$\sigma_D = \frac{\pi}{4} d_{LT}^2 \quad \sigma_E = \frac{\pi}{4} d_{LNT}^2$$

$$m_D = 2000 \frac{\pi}{6} d_{LT}^3 \quad m_E = 2000 \frac{\pi}{6} d_{LNT}^3$$

3.1 Collision Rate

The fragmenting and non-fragmenting collision rates, \mathcal{F}_Y and \mathcal{G}_Y (collisions $\cdot \text{s}^{-1}$), respectively, for $X \in \{A, C, P, Q, R, D, E\}$ are modeled as:

$$\mathcal{F}_X = \mathbf{w} \circ \left[\sum_{Y \in \{A,C,P,Q,R,D,E\}} F_{XY} \theta_{XY} \sigma_{XY} \mathbf{Y} \right] \circ \mathbf{X}$$

$$\mathcal{G}_X = \mathbf{w} \circ \left[\sum_{Y \in \{A,C,P,Q,R,D,E\}} (1 - F_{XY}) \theta_{XY} \sigma_{XY} \mathbf{Y} \right] \circ \mathbf{X}$$

where \mathbf{X} and \mathbf{Y} are placeholders for the $N \times 1$ state vectors and \circ denotes the Hadamard (elementwise) product.

F_{XY} is an indicator variable that indicates if collisions between objects of class X and objects of class Y are fragmenting. We assume that fragmentation occurs if the specific energy of the collision exceeds 40 J/g [19], where relative collision velocity is approximated as 1.32 times the orbital velocity (assuming the crossing orbits are uniform over inclination, RAAN, and mean anomaly). Namely,

$$F_{XY} = \begin{cases} 1 & \min(m_X, m_Y) > \max(m_X, m_Y) / 1318 \\ 0 & \text{otherwise} \end{cases}$$

The collision coefficient between objects of type Y and X is given by

$$\theta_{XY} = \begin{cases} 2\alpha^2 & X \in \{A, C\} \wedge Y \in \{A, C\} \\ \alpha & (X \in \{A, C\} \vee Y \in \{A, C\}) \wedge (X \neq E \wedge Y \neq E) \\ 2 & X = Y \wedge X \notin \{A, C\} \\ 1 & \text{otherwise} \end{cases}$$

This coefficient accounts for active object collision avoidance and for collisions of objects from the same class destroying two objects.

The effective collision area (m^2) for each object type pair is modeled as

$$\sigma_{XY} = \sigma_X + \sigma_Y$$

3.1.1 Collision Flux

Assuming that the orbits of the objects in each shell are independent and identically distributed uniformly over inclination, RAAN, and mean anomaly, the $N \times 1$ collision flux vector ($\text{m}^{-2} \cdot \text{s}^{-1} \cdot \text{objects}^{-2}$) is

$$\mathbf{w} = \begin{bmatrix} \frac{v_1}{V_1} \\ \vdots \\ \frac{v_N}{V_N} \end{bmatrix}$$

The mean collision velocity ($\text{m} \cdot \text{s}^{-1}$) in shell k is approximated as 1.32 times the orbital velocity (consequence of the uniform over inclination, RAAN, and mean anomaly assumption) and given by

$$v_k = 1.32 \sqrt{\frac{\mu}{R_e + h_k}}$$

where $\mu = 3.986004418 \times 10^{14} \text{ m}^3 \cdot \text{s}^{-2}$ and $R_e = 6.378137 \times 10^6 \text{ m}$.

The volume (m^3) of the k^{th} shell is

$$V_k = \frac{4\pi}{3} \left[\left(R_e + h_k + \frac{\Delta h}{2} \right)^3 - \left(R_e + h_k - \frac{\Delta h}{2} \right)^3 \right]$$

3.2 Debris Creation Rate

The LT and LNT debris creation rates (objects \cdot s⁻¹) are given by the following equations, respectively.

$$\mathbf{C}_{LT} = \mathbf{w} \circ \left[\sum_{X \in \{A, C, P, Q, R\}} \left[\sum_{\substack{Y \in \{A, C, P, Q, R, D, E\} \\ Y \leq X}} F_{XY} \eta_{XY} \psi_{XY} \sigma_{XY} Y \right] \circ \mathbf{X} \right]$$

$$\mathbf{C}_{LNT} = \beta \mathbf{C}_{LT} + \mathbf{w} \circ [\eta_{DD} \sigma_{DD} \mathbf{D} + \eta_{DE} \sigma_{DE} \mathbf{E}] \circ \mathbf{D}$$

Solely for purposes of the summation indexing, $A > C > P > Q > R > D > E$.

The object creation coefficient, which account for active satellite collision avoidance, is given by

$$\psi_{XY} = \begin{cases} \alpha^2 & X \in \{A, C\} \wedge Y \in \{A, C\} \\ \alpha & (X \in \{A, C\} \vee Y \in \{A, C\}) \wedge (X \neq E \wedge Y \neq E) \\ 1 & \text{otherwise} \end{cases}$$

Following the NASA Standard Breakup Model [19], the ratio of LNT fragments to LT fragments is

$$\beta = \left(\frac{d_{LNT}}{d_{LT}} \right)^{-1.71} - 1$$

A mass conserving model is used for the number of objects, η_{XY} , resulting from a collision

$$\eta_{XY} = \begin{cases} \frac{m_X + m_Y}{m_E} & X \in \{D, E\} \wedge Y \in \{D, E\} \\ \frac{m_X + m_Y}{m_D + \beta m_E} & \text{otherwise} \end{cases}$$

3.3 State Vector Evolution

Evolution of the state vectors is modeled using the following system of non-linear vector differential equations:

$$\frac{\partial \mathbf{A}}{\partial t} = \frac{1}{\zeta} \mathbf{a} - \frac{1}{\zeta} \mathbf{A} - \mathcal{F}_A - \mathcal{G}_A$$

$$\frac{\partial \mathbf{C}}{\partial t} = \frac{1}{\zeta} \mathbf{c} - \frac{1}{\zeta} \mathbf{C} - \mathcal{F}_C - \mathcal{G}_C$$

$$\frac{\partial \mathbf{P}}{\partial t} = \frac{(1-\rho)}{\zeta} \mathbf{A} - \Phi[\mathbf{d}_P \circ \mathbf{P}] - \mathcal{F}_P + \mathcal{G}_A$$

$$\frac{\partial \mathbf{Q}}{\partial t} = \frac{(1-\rho)}{\zeta} \mathbf{C} - \Phi[\mathbf{d}_Q \circ \mathbf{Q}] - \mathcal{F}_Q + \mathcal{G}_C$$

$$\frac{\partial \mathbf{R}}{\partial t} = -\Phi[\mathbf{d}_R \circ \mathbf{R}] - \mathcal{F}_R$$

$$\frac{\partial \mathbf{D}}{\partial t} = -\Phi[\mathbf{d}_D \circ \mathbf{D}] - \mathcal{F}_D + \Theta \mathbf{C}_{LT}$$

$$\frac{\partial \mathbf{E}}{\partial t} = -\Phi[\mathbf{d}_E \circ \mathbf{E}] - \mathcal{F}_E + \Theta \mathbf{C}_{LNT}$$

The vector \mathbf{c} is the number of satellites launched over time ζ to probe RCC. The satellites launched over time ζ to model competing consumers of RCC are represented by \mathbf{a} . The satellites present at initialization are not replenished. Adapting the finite-time RCC (Section 2) to the model, gives

$$\tilde{\mathbf{C}}^* = \max_{\mathbf{c}} \tilde{\mathbf{C}}_{eq} \quad \text{subject to} \quad \mathbf{c}(1 - \delta) \leq \tilde{\mathbf{C}}_{eq}$$

where maximization is performed per element with all the other elements set to zero. It is approximated by varying the probe size from 100 satellites to 1 million satellites with a 1 dB step size and identifying the largest probe size that can be maintained for 100 years within the above constraint. The resulting error bound on the RCC maximization is -11%/+12%. As above, δ , is the replacement rate constraint for satellites rendered non-operational or fragmented by collisions,

The first term in the equations for active satellites (A and C) models the satellite launches, the second term the decay over lifetime, the third term the destruction of satellites in fragmenting collisions, and the fourth term the conversion of active satellites to passive satellites through non-fragmenting collisions. The first term for the passive satellites (P and Q) models the conversion of active satellites into passive satellites at end of life due to PMD failure, the second term the decay of passive satellites from higher orbits and into lower orbits, the third term the destruction of passive satellites through collisions, and the fourth term the increase in passive satellites due to non-fragmenting collisions of active satellites. For the derelict rocket bodies (R), the first term models the decay from higher orbits and into lower orbits, and the second term the destruction of rocket bodies through collision. The first term for the debris (D and E), models the decay from higher orbits and into lower orbits, the section term the destruction due to collisions, and the final term, the creation of debris from fragmenting collision.

The $N \times N$ state decay transition matrix Φ models exiting a shell by decay to the next lower shell and entering a shell by decay from the shell above. The active satellites (A and C) are assumed to station-keep, and hence do not decay.

$$\Phi = (\mathbf{I} - \mathbf{U}_N) = \begin{bmatrix} 1 & -1 & 0 & \dots & 0 & 0 & 0 \\ 0 & 1 & -1 & \dots & 0 & 0 & 0 \\ 0 & 0 & 1 & \dots & 0 & 0 & 0 \\ \vdots & \vdots & \vdots & \ddots & \vdots & \vdots & \vdots \\ 0 & 0 & 0 & \dots & 1 & -1 & 0 \\ 0 & 0 & 0 & \dots & 0 & 1 & -1 \\ 0 & 0 & 0 & \dots & 0 & 0 & 1 \end{bmatrix}$$

The decay rate vectors (\mathbf{d}_X) are discussed in Section 3.3.1 and the collision coupling matrix (Θ), which quantifies the distribution of collision fragments over the orbital shells around the shell in which the collision occurred, in Section 3.3.2.

3.3.1 Decay Rate

The $N \times 1$ decay rate vectors $\mathbf{d}_P, \mathbf{d}_Q, \mathbf{d}_R, \mathbf{d}_D, \mathbf{d}_E$ (shells \cdot s $^{-1}$) are given by

$$\mathbf{d}_X = \begin{bmatrix} \gamma_{X_1} \\ \varphi_1 \\ \vdots \\ \gamma_{X_N} \\ \varphi_N \end{bmatrix}$$

The fraction of a shell that drag reduces the altitude per orbit, γ_{X_k} , is

$$\gamma_{X_k} = \begin{cases} \frac{-2\pi(R_e + h_k)^2 \rho_k c_d \sigma_X / m_X}{\Delta h} & h_k \leq 1,000,000 \text{ m} \\ 0 & \text{otherwise} \end{cases}$$

where ρ_k is the atmospheric density ($\text{kg} \cdot \text{m}^{-3}$) in shell k and c_d is the coefficient of drag (typically 2 to 2.2) [20].

The orbital period (s) in shell k is

$$\varphi_k = \frac{2\pi}{\sqrt{\frac{\mu}{(R_e + h_k)^3}}}$$

3.3.2 Collision Coupling

The NASA Standard Breakup Model [19] is used to determine the distribution of collision fragments over the orbital shells. The $N \times N$ collision coupling matrix models the altitude spread of debris following a collision

$$\boldsymbol{\theta} = [\theta_{j,k}]$$

The fraction of fragments that couple from a collision in shell j to shell k is given by

$$\theta_{j,k} = a_j e^{b_j |h_j - h_k|}$$

where $b_j = 3.854 \times 10^{-12} \times h_j - 2.334 \times 10^{-5}$ and $a_j = \left(2 \frac{e^{b_j \Delta h}}{1 - e^{b_j \Delta h}} + 1\right)^{-1}$.

The constants in the equation for b_j were determined by fitting to the altitude spread calculated using the NASA Standard Breakup Model [19]. The a_j were chosen to conserve mass from a fragmenting collision across all altitudes, thus debris that would have a mean altitude below the lowest shell or above the highest shell are ignored.

4. PARAMETERS

The fixed parameters are summarized in Tab. 1. The start year is used to determine the solar flux at each time step, which is used to compute the atmospheric density in Section 3.3.1. A 100-year duration was selected to focus on near-term (in a cosmic sense) events and is used as the RCC time limit. The time step was selected to provide reasonable simulation times with fixed time step integration while providing the same RCC results compared to the Runge-Kutta-Fehlberg method (RKF45) which uses a variable step size with error control [21].

The characteristic lengths of LT debris (d_{LT}) is the commonly used 0.1 m. For LNT debris (d_{LNT}), 0.03 m is used. With these assumptions, the masses are 1.05 kg and 0.028 kg, respectively, and the fragmentation thresholds are 1,380 kg and 37.3 kg, respectively. Objects more massive than 1,380 kg will not be fragmented by collisions with LT debris and those more massive than 37.3 kg will not be fragmented by collisions with LNT debris.

The mass and cross-sectional area of the active satellites (m_A and σ_A) and derelict rocket bodies (m_R and σ_R) are set to the average values for the LEO satellites and the derelict rocket bodies currently in orbit [2]. Using the average values ensures that the total number, total mass, and total cross-sectional area of the satellites and rocket bodies are properly initialized. We assume that no new derelict rocket bodies are created.

Tab. 1 – Fixed Parameters

Parameter	Value	Parameter	Value
Start Year	2022	d_{LT}	0.1 m
Time Step	1 day	d_{LNT}	0.03 m
T	100 years	m_A	366 kg
δ	0.1	σ_A	6.3 m ²
Δh	25,000 m	m_R	1,445 kg
c_d	2.2	σ_R	11.8 m ²

Tab. 2 lists the probe satellite parameter values for representative capacity cases—High, Middle, and Low. The ODMSP [6] requires that large constellation satellites have a 90% probability of successful post mission disposal with a goal of 99%. Large constellation satellites design lifetimes typically range from 5 to 10 years [22].

Ranges for the satellite mass and cross-sectional area are based on those of objects currently in orbit and those reported for new large- constellation satellites. The newer first-generation SpaceX satellites have 260 kg mass and 27.6 m² max cross-sectional area [23]. It has recently been suggested that second-generation SpaceX satellites will have 2,000 kg mass and 294 m² [24]. First-generation OneWeb satellites are 148 kg and 5.3 m² [23].

Tab. 2 – Cases

Parameter	High Case	Middle Case	Low Case
ρ	0.99	0.95	0.90
α	10 ⁻⁶	10 ⁻⁵	10 ⁻⁴
ζ	10 years	7 years	5 years
σ_c	10 m ²	20 m ²	40 m ²
m_c	50 kg	250 kg	1,250 kg

The area-to-mass ratios (A/M) for these cases are 0.2, 0.08, and 0.032 (m² · kg⁻¹), respectively. The relative masses are such that for all three cases, active satellites are converted to passive by collisions with LNT debris, and active and passive satellites, rocket bodies, and LT debris are fragmented by collisions with LT debris, as well as with each other.

5. RESULTS

The model developed in Section 3 was evaluated using the parameters in Section 4. Fig. 3 shows the RCC for two cases—where the state vectors are initialized with the SATCAT objects, and where they are initialized to zero, empty space. As expected, the carrying capacity in terms of number of satellites is highest for the High case and lowest for the Low case. Comparing the Empty Space case with the SATCAT case, the most pronounced effects correspond to the higher altitude mass and cross-sectional area peaks. Note that the slight RCC increase at the higher altitudes is due to lower collision risk with larger shell volume and the model truncating space at 2,000 km.

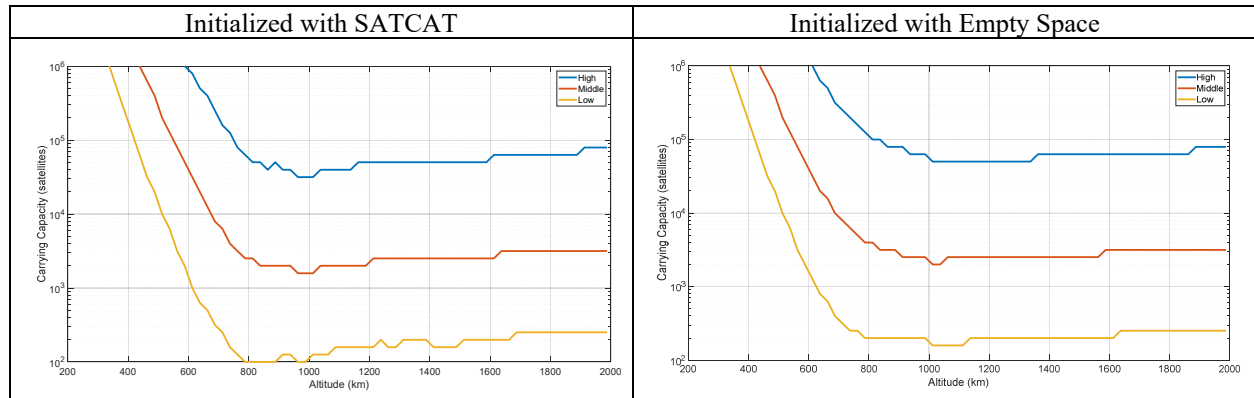


Fig. 3 – RCC Cases

The impact of the derelict rocket body bodies is isolated in Fig. 4 where the left panel shows the RCC with the full SATCAT initialization and the right panel shows the RCC with the derelict rocket bodies removed. While the rocket body impact is readily observable, it is also significantly less than an order of magnitude, relatively small compared to some of the following parameter sensitivities.

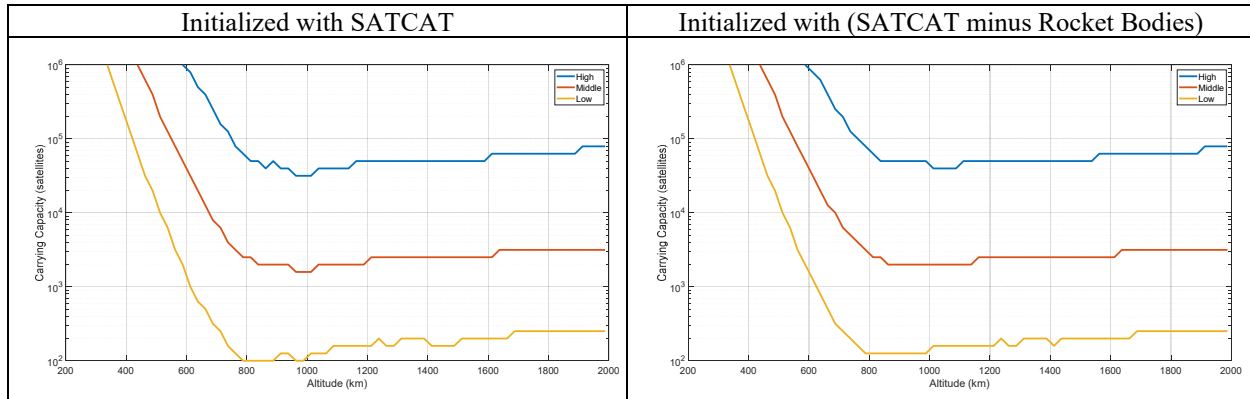


Fig. 4 – RCC Sensitivity to Derelict Rocket Bodies

The significant impact of maneuverability is shown in Fig. 5. The panel on the left shows the baseline cases while that on the right shows the capacity with 0% satellite reliability (no PMD) and 100% avoidance failure rate. The reduction in RCC is over an order of magnitude, with only the region below 400 km supporting significant capacity without maneuverability, due to the increased drag in that region leading to relatively rapid decay of even passive, non-maneuverable satellites.

The decrease in RCC can, in large part, be explained by the accumulation of passive satellites which are then converted into debris. This effect is more severe at higher altitudes where atmospheric drag is negligible, meaning that passive satellites are only removed when they are converted into debris within the RCC limit time. At lower altitudes, many of the passive satellites re-enter the atmosphere rather than being converted into debris—decreasing the rate of growth of debris and increasing the RCC. A more detailed description of the impact of reliability is performed later in this section.

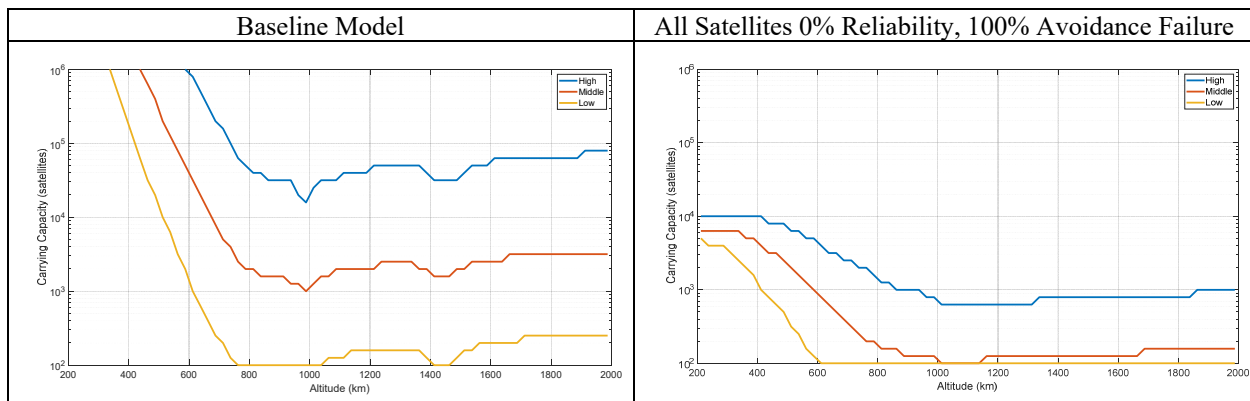


Fig. 5 – RCC Sensitivity to Satellite Maneuverability (Initialized with SATCAT)

Fig. 6 shows that there is some improvement in RCC as the replacement rate constraint for satellites rendered non-operational or fragmented by collisions, δ , is increased from 5% to 20%. However, the improvement only approaches significance near the 1,000 km mass/cross-section peak with the SATCAT initialization. This indicates that RCC is relatively insensitive to the choice of δ , so long as the value is not too close to zero. As δ approaches zero, so does the carrying capacity. If satellites are only launched at exactly the rate other satellites in the constellation reach end-of-life, then even one loss due to a collision will prevent sustaining the constellation size.

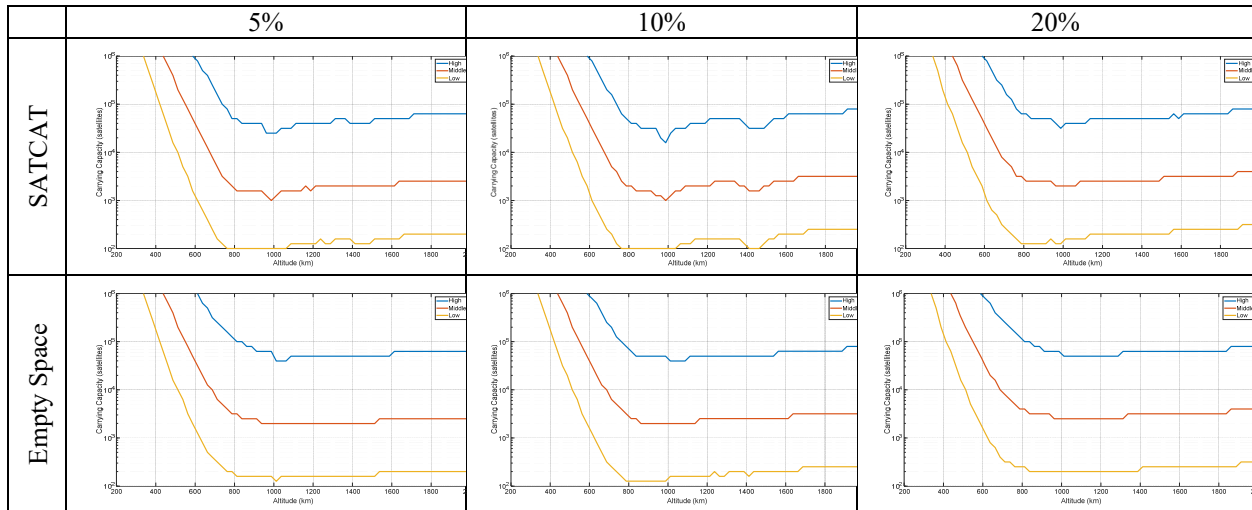


Fig. 6 – RCC Cases Sensitivity to Replacement Rate

5.1 Sensitivity to Satellite Parameters

Sensitivity analysis was performed with respect to each of the case parameters (ρ , α , ζ , σ_c , m_c) individually around the Middle case with initialization to the SATCAT and with initialization to empty space.

5.1.1 Reliability Sensitivity

Fig. 7 shows the sensitivity to satellite reliability (ρ). With the Middle case 10^{-5} collision avoidance failure rate, α , 0% PMD only provides significant RCC below 600 km, compared to the 400 km value with 100% collision avoidance failure rate and 0% PMD. At the higher altitudes, a roughly one order of magnitude increase in RCC is seen when increasing PMD from 90% to 99%. With 100% PMD, the initialized to empty space case has $\gg 10^6$ RCC at all altitudes over the 100 years. This is to be expected as with the Empty Space initial condition, there are no debris that could disable active satellites, and a 100% PMD rate means that no passive satellites accumulate. The only way for debris to be formed is through collisions between two active satellites, which has probability $\alpha^2 < 10^{-10}$. When initialized with the SATCAT, the 100% PMD case is like the 99% case in regions with significant initial mass and cross-sectional area, and significantly larger in regions with low initial mass and cross-sectional area.

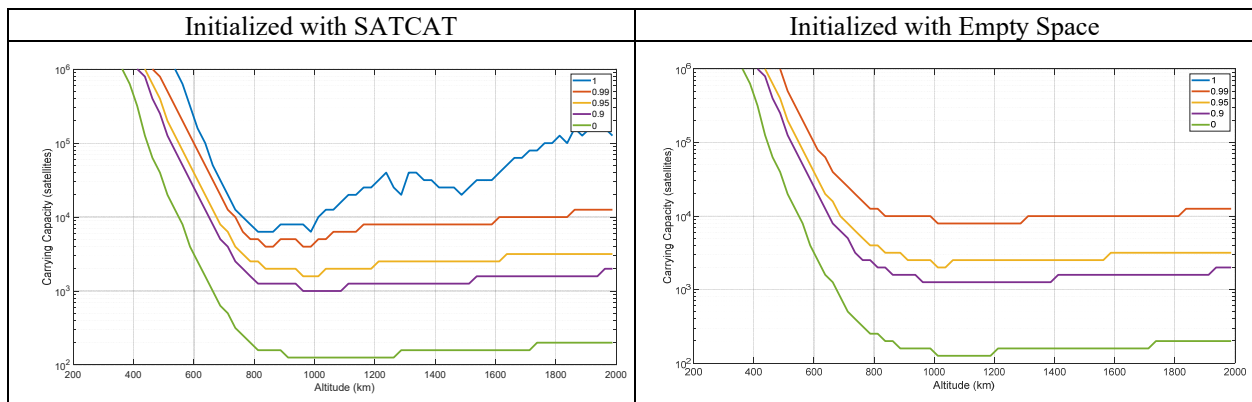


Fig. 7 – RCC Sensitivity to Satellite Reliability

5.1.2 Avoidance Failure Sensitivity

Sensitivity to active satellite collision avoidance failure probability, α , is shown in Fig. 8. The two initialization conditions provide similar results, with the larger variations around the mass and cross-sectional area peaks. Above

around 700 km is almost an order of magnitude improvement going from 100% collision avoidance failure rate to 10%, and then no significant benefit reducing collision avoidance failure rate further. Below 700 km, there is some additional benefit improving the collision avoidance failure rate to 1%, but then no further benefit beyond that. With the 95% PMD rate of the Middle case, the 100% collision avoidance failure rate only provides significant RCC below 600 km.

This result is to be expected as the loss of active satellites is dominated in the high debris limit (which is reached near capacity) by

$$\mathcal{F}_A + \mathcal{G}_A \approx \alpha \sigma_{AD} wAD + \sigma_{AE} wAE$$

where drag is negligible, and neglecting collisions between the debris, we have $E \approx \beta D$. Approximating σ_{AD} and σ_{AE} as σ_A gives

$$\mathcal{F}_A + \mathcal{G}_A \approx \sigma_A (\alpha + \beta) wAD$$

For the parameters given in Section 4, we have

$$\beta = \left(\frac{0.03}{0.1} \right)^{-1.71} - 1 = 6.83651$$

which dominates α .

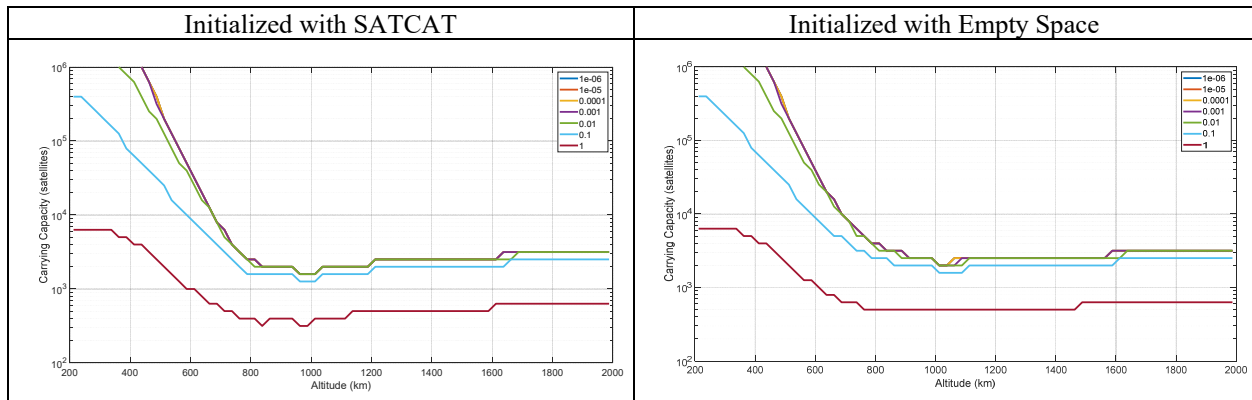


Fig. 8 – RCC Sensitivity to Active Satellite Collision Avoidance Failure Probability

5.1.3 Lifetime Sensitivity

Fig. 9 shows that RCC is relatively insensitive to satellite lifetime. This is not surprising as in the model, the launch rate is reduced by a factor of the satellite lifetime. In general, longer satellite lifetimes result in a slower accumulation of debris as fewer passive satellites are left in orbit because of failed disposal of satellites with shorter lifetime. Therefore, a longer lifetime leads to an increased RCC.

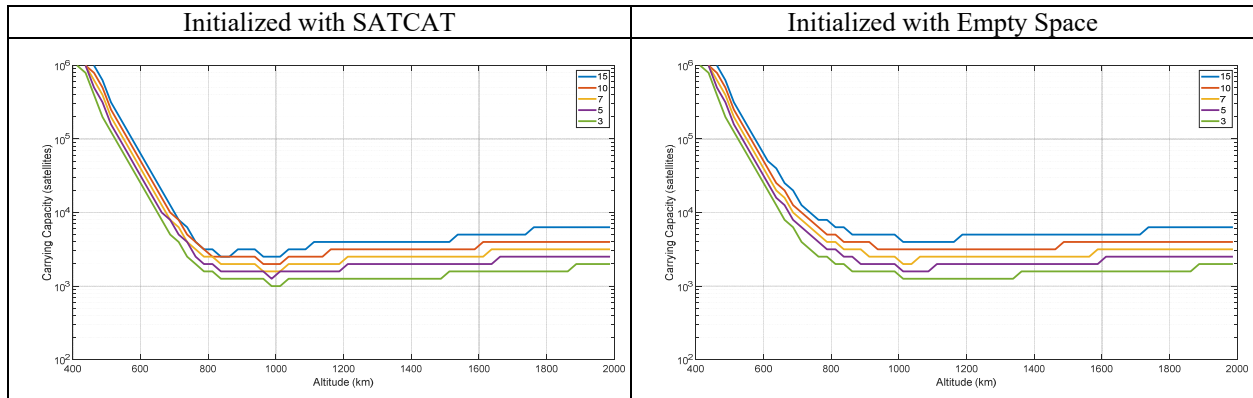


Fig. 9 – RCC Sensitivity to Satellite Lifetime

5.1.4 Mass Sensitivity

The sensitivity to satellite mass is shown in Fig. 10. The A/M is held constant, adjusting the cross-sectional area as a function of mass to maintain the Middle case value of $0.08 \text{ m}^2 \cdot \text{kg}^{-1}$. This eliminates sensitivity to passive satellite decay rate. The 50 kg, 250 kg, and 1,250 kg cases have the behavior that active satellites are converted to passive by collisions with LNT debris and are fragmented by collisions with LT debris. For the 10 kg case, as per our model, the active satellites are also fragmented by collisions with LNT debris, while for the 6,250 kg case, the active satellites are never fragmented by collisions with debris, only converted to passive.

For constant A/M ratio, and the other Middle case parameters (95% PMD success, 10^{-5} probability of active satellite collision avoidance failure, and 7-year lifetime), less massive satellites provide significantly higher RCC. Even though the 10 kg satellites are fragmented by LNT debris, they still provide higher RCC than all the other cases above 600 km, until they cross the 50 kg case near 1 million satellites RCC. The only region where a significant number of satellites over 1 metric ton could potentially be deployed is below 600 km.

Increasing satellite mass decreases the RCC as each collision produces more LT and LNT debris (η_{XY} is proportional to the sum of the masses of the objects). With constant A/M , the cross-sectional area also varies with the satellite mass. The primary effect of which is increasing the rate at which active satellites are converted to passive satellites, as the non-fragmenting collision rate is

$$\sigma_{AE}wAE \approx \sigma_AwAE \propto \sigma_A$$

which dominates the fragmenting collision rate for active satellites. The secondary effect is an increase in the LT and LNT debris populations because of collisions between passive satellites and other passive satellites or LT debris, the rate of which is increased due to the increased number of passive satellites and the increased cross-sectional area of those satellites. This severity of this second effect is limited when atmospheric drag causes the passive satellites to decay, hence the difference is less pronounced below 700 km.

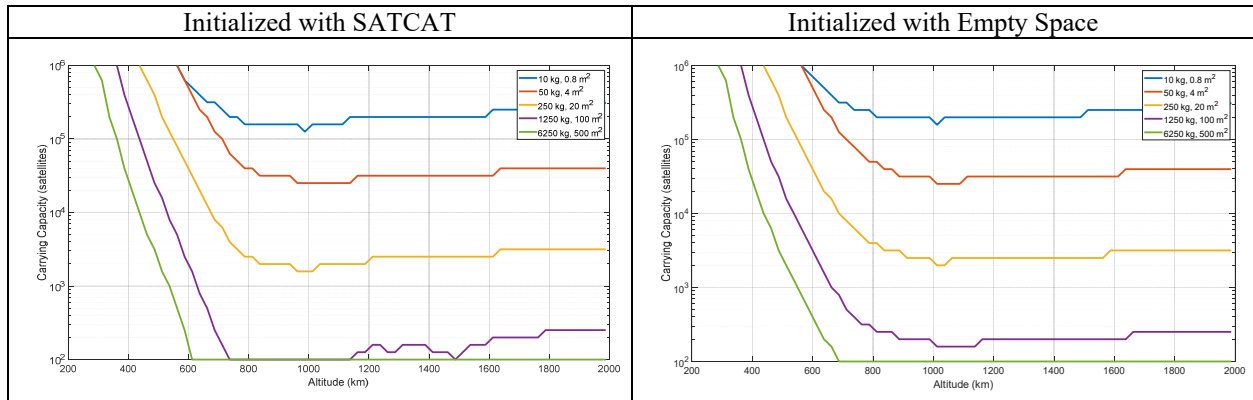


Fig. 10 – RCC Sensitivity to Satellite Mass (kg) with Constant A/M ($\text{m}^2 \cdot \text{kg}^{-1}$)

5.2 Sensitivity to Constellations Competing for RCC

The impact of constellations competing for RCC relative to empty space is illustrated in Fig. 11. The RCC with the first and second generation NGSO configurations from SpaceX (4,408 and 29,988 satellites, respectively) and OneWeb (716 and 6,372 satellites, respectively) are compared to the empty space RCC for the Middle case. The Middle case parameters are used for the probe and all satellites (probe and constellations competing for RCC) are modeled with the Middle case’s 95% PMD success, 10^{-5} collision avoidance failure, and 7-year lifetime. The mass and cross-sectional area values noted above were used for the Starlink satellites and the first-generation OneWeb satellites. As no reliable information was available for the second-generation OneWeb satellites, the first-generation values were used for the satellites in the 6,372-satellite second-generation constellation.

The first-generation configurations (using the specified satellite characteristic and quantities) are seen to have little impact on RCC relative to empty space, their curves are overlaid by the Empty Space curve. However, the second-generation systems have a very substantial impact. The second-generation SpaceX configuration effectively consumes all the Empty Space RCC from 400 km to 750 km, and reduces RCC at 850 km, more than 200 km above its nominal highest altitude shell (614 km). This is an example of the non-local consequences of large constellation deployments in LEO, as modeled by the coupling matrix in the model. The second-generation OneWeb configuration is a second example, reducing RCC over a 200 km region around its nominal 1,200 km orbital shell. At 1,200 km, the second-generation OneWeb configuration consumes 75% of the Empty Space RCC.

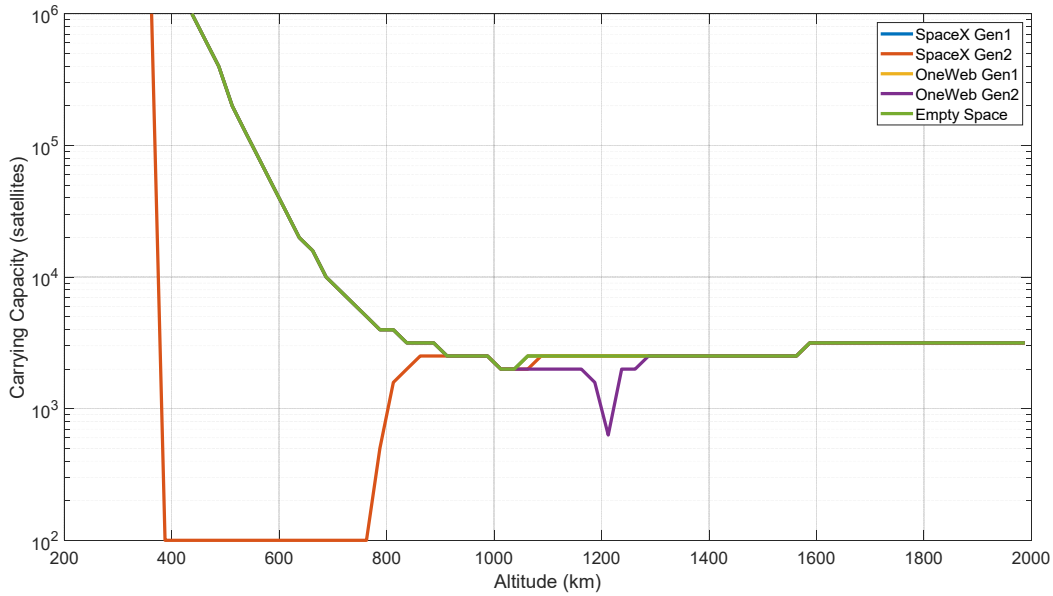


Fig. 11 – Comparison of RCC with First and Second Generation NGSO Systems from SpaceX and OneWeb (Initialized with Empty Space)

6. CONCLUSION

We have developed a holistic model and used it to explore the sensitivity of finite time RCC to various initial conditions, parameters, and constellations competing for capacity. The results generated are based on the model, underlying assumptions, and inputs; and any conclusions drawn are limited as such. We have several interesting results. First, removing the existing population of derelict rocket bodies does not appear to have a material impact on RCC. Second, at least for one reasonable scenario, the Middle case, reducing active satellite collision avoidance failure rate to better than 10^{-1} (better than 10^{-2} below 700 km) provides limited benefit. Note that this is the failure of avoiding what would have been an actual collision, conditioned on both objects being trackable, regardless of the cause of the failure—SST or STM.

Third, when varying mass and cross-sectional area to maintain constant A/M along with the other Middle case assumptions (95% PMD success, 10^{-5} probability of active satellite collision avoidance failure, and 7-year lifetime), we find that less massive, lower area satellites provide significantly higher RCC. Even though CubeSat sized satellites may be fragmented by LNT debris, they still provide higher RCC than more massive satellites at least until the RCC approaches 1 million CubeSats. With the Middle case A/M of $.08 \text{ m}^2 \cdot \text{kg}^{-1}$, the only LEO region where significant numbers of satellites over 1 metric ton could be deployed is below 600 km.

Another interesting result is that relative to initialization with empty space, the first-generation SpaceX and OneWeb systems do not exhibit a significant reduction in carrying capacity (less than the resolution of the probes, i.e., no greater than 11%). The second-generation versions of these systems do reduce or eliminate RCC in some orbits, with the second-generation SpaceX configuration consuming 100% of the Empty Space RCC between 400 km and 750 km, and the second-generation OneWeb configuration reducing Empty Space RCC at 1200 km by 75%. Both second-generation configurations also exhibit non-local consequences, i.e., constellations deployed at one altitude, or band of altitudes, that meaningfully reduces RCC at neighboring altitudes.

As noted in Section 1, an earlier study [5] estimated the carrying capacity as 40,000 satellites at 600 km altitude and 1,000 satellites at 1,200 km. The parameters used in that study are like our Middle case parameters. From Fig. 3, the estimated RCC is 40,900 satellites at 600 km and 2,250 satellites at 1,200 km. Given the differences in assumptions, these results tend to confirm each other.

Potential policy implications of these results include:

- a) Managing the number of satellites, mass, and cross-sectional area launched into different orbits (admittance control) is fundamental to sustainability, as is the reliability (probability of PMD) of those satellites.
- b) Investing in large debris removal (rocket bodies) may not have a significant impact on long term (100 year) sustainability.
- c) Altitudes below 400 km may be suitable for non-propulsive satellites.
- d) Altitudes in the 400 km to 600 km range may be suitable for mega-constellations, provided that the number of satellites, mass, and cross-sectional area launched are managed.
- e) Smaller constellations above 600 km are likely sustainable depending on mass and cross-sectional area.

We have provided an approach to better estimate future debris propagation using a RCC metric that enables comparing holistic global contributions to debris propagation as a function of specific system characteristics and deducing the incremental impact of individual systems and characteristics on LEO carrying capacity. Future work will extend these results in two ways. First, by evaluating the potential RCC available after various other proposed configurations, and combinations of these configurations are deployed. Second, by improving fidelity through improved orbit and collision models with even more comprehensive state vectors.

7. REFERENCES

- [1] FCC, Mitigation of Orbital Debris in the New Space Age Mitigation of Orbital Debris, *Notice of Proposed Rulemaking*, 33 FCC Rcd 11352 (17), released Nov 19, 2018.
- [2] ESA Space Debris Office, *ESA's Annual Space Environment Report*, EN-DB-LOG-00288-OPS-SD, Issue/Revision 6.0, 22 April 2022.
https://www.sdo.esoc.esa.int/environment_report/Space_Environment_Report_latest.pdf
- [3] ITU, *e-Submission of Satellite Network Filings*, <https://www.itu.int/ITU-R/space/asreceived/Publication/AsReceived>
- [4] D. J. Kessler and B. G. Cour-Palais, Collision Frequency of Artificial Satellites: The Creation of a Debris Belt. *Journal of Geophysical Research*. 83 (A6): 2637–2646, 1978.
- [5] G. Long, *The Impacts of Large Constellations of Satellites*, JASON – The MITRE Corporation, JSR-20-2H, November 2020, (Updated: January 21, 2021).
- [6] U.S. Government, *Orbital Debris Mitigation Standard Practices*, November 2019 Update.
- [7] M. Twain, *Life on the Mississippi*, James R. Osgood & Co., Boston. 1883.
- [8] P. Anker. "The ecological colonization of space." *Environmental History* 10, no. 2 (2005): 239-268.
- [9] A. V. Gheorghe and D. E. Yuchnovicz, The space infrastructure vulnerability cadastre: Orbital debris critical loads. *International Journal of Disaster Risk Science*, 6(4), 359-371. 2015.
- [10] S. Rouillon, 2019. "A physico-economic model of space debris management," Cahiers du GREThA (2007-2019) 2019-10, *Groupe de Recherche en Economie Théorique et Appliquée (GREThA)*.
- [11] E. Cirkovic, M. Rathnasabapathy, and D. Wood. "Sustainable orbit and the Earth system: mitigation and regulation." *Proc. 8th Conference on Orbital Space Debris*. 2021.
- [12] H. G. Lewis, and N. Marsh. "Deep Time Analysis of Space Debris and Space Sustainability." *Proc. 8th European Conference on Space Debris*. 2021.
- [13] R. Buchs, Collision risk from space debris: Current status, challenges and response strategies. Lausanne: EPFL *International Risk Governance Center*. 2021.
- [14] A. Lawrence, M. L. Rawls, M. Jah, *et al.* The case for space environmentalism. *Nat Astron* 6, 428–435 (2022).
<https://doi.org/10.1038/s41550-022-01655-6>
- [15] L. Miraux, Environmental limits to the space sector's growth, *Science of The Total Environment*, Volume 806, Part 4, 2022.
- [16] F. Letizia, B. Bastida Virgili, and S. Lemmens, *Assessment of environmental capacity thresholds through long-term simulations*, <https://www.sciencedirect.com/science/article/abs/pii/S0273117722004793?via%3Dihub>
- [17] European Space Policy Institute (ESPI), "Space Environment Capacity: Policy, regulatory and diplomatic perspectives on threshold-based models for space safety & sustainability", April 2022,
<https://www.espi.or.at/wp-content/uploads/2022/06/ESPI-Report-82-Space-Environment-Capacity-Full-Report.pdf>
- [18] Space-Track.org, <https://www.space-track.org/#catalog> (data updated 5 July 2022).

- [19] A. Horstmann, S. Hesselbach, C. Wiedemann, S. Flegel, and M. Oswald, Final Report – Enhancement of S/C Fragmentation and Environment Evolution Models. DD-0045, *Institute of Space Systems*, Technische Universität Braunschweig, 2020.
- [20] D. A. Vallado, *Fundamentals of Astrodynamics and Applications*, Fourth Edition, Microcosm Press, 2013.
- [21] Fehlberg, E. Low-Order Classical Runge-Kutta Formulas with Step-size Control and Their Application to Some Heat Transfer Problems; *National Aeronautics and Space Administration*: Washington, DC, USA, 1969; Volume 315.
- [22] M. A. Sturza, and G. Saura Carretero. "Design Trades for Environmentally Friendly Broadband LEO Satellite Systems." In *2021 Advanced Maui Optical and Space Surveillance Technologies Conference (AMOS)*. 2021.
- [23] ESA, DISCOSweb (data updated 5 July 2022), <https://discosweb.esoc.esa.int/objects>
- [24] SpaceX, Letter to Marlene H. Dortch, Secretary, Federal Communications Commission, re IBFS File Nos. SAT-LOA-20200526-00055 and SAT-AMD-20210818-00105, 19 August 2022.